Magnesium Technology 2011
Edited by: Wim H. Sillekens, Sean R. Agnew, Neale R. Neelameggham, and Suveen N. Mathaudhu
TMS (The Minerals, Metals & Materials Society), 2011

TEXTURE WEAKENING EFFECT OF Y IN Mg-Zn-Y SYSTEM

S. A. Farzadfar[1], M. Sanjari[1], I.-H. Jung[1], E. Essadiqi[2] and S. Yue[1]

[1]McGill University, Department of Materials Engineering, Montreal, QC, Canada H3A 2B2
[2]CANMET- Materials Technology Laboratory, Ottawa, Ontario, Canada K1A 0G1

Keywords: Magnesium, Yttrium, Compression test, Thermodynamics, Texture

Abstract

The CALPHAD (Calculation of Phase Diagram) method was successfully used in this study to select the alloys from Mg-Zn-Y system, aimed at determining the mechanism(s) of texture weakening in Y-containing Mg alloys: PSN (particle-stimulated nucleation of recrystallization) and/or solute effects. The selected alloys are Mg-6Zn-1.2Y, Mg-5Zn-2Y, Mg-2.9Y and Mg-2.9Zn (in wt%). After heat treatment, the ternary alloys contain (nearly) the same amount of ternary intermetallics in equilibrium with α-Mg at 350 °C, and the microstructure of the binary alloys is composed of α-Mg solid solution at 350 °C containing the same solute amount as that in the ternary alloys. The hot deformation and post-deformation annealing of these alloys at a constant temperature (i.e., 350 °C) showed that the texture weakening happens during growth of recrystallized grains in deformed and annealed samples where Y element is in α-Mg solid solution.

Introduction

The use of wrought Mg alloys, and especially flat-rolled sheets, in industrial applications is still limited mainly due to their low formability [1]. This poor formability is a direct consequence of the development of the basal texture upon deformation, resulting in plastic anisotropy and tension-compression asymmetry [2-4]. However, it has recently been found that the addition of rare earth (RE) elements, such as yttrium (Y), significantly weakens the deformation texture [3-4, 5, 6, 7], e.g., after multi-pass rolling, or the annealed texture [6, 8, 9]. To date, the mechanism(s) of texture weakening, which are most likely connected with the presence (or absence) of intermetallics and/or solutes, are not well understood. There is practically no systematic work on RE-containing Mg alloys with controlled levels of solutes and precipitates during deformation and annealing that allows for separating the possible mechanisms of texture weakening. The objective of this study is therefore to perform systematic alloy selection by CALPHAD (Calculation of Phase Diagram) method and FactSage™ software [10] to clarify the mechanisms involved in texture weakening after hot deformation of the selected alloys.

Alloy Selection

The Mg-Zn-Y system was chosen as the alloy system in this study firstly because of the reported texture weakening observed in this system [2, 5, 8, 11], and secondly because of the large solubility of Zn or Y in Mg as compared to other elements such as Mn, La, Ce or Nd [12, 13]. There is also the possibility of generating two-phase microstructures (α-Mg + ternary intermetallic) with different types of intermetallics. Since equilibrium state at deformation temperature is desired, the temperature of deformation and therefore that of thermodynamic calculations must first be determined. Based upon the typical temperature range in industrial processes such as rolling, i.e., 300 °C to 450 °C [14], the temperature of 350 °C was chosen in this study. Two categories of alloys with the following microstructures at 350 °C were selected: (a) two-phase microstructure Mg-Zn-Y alloys with the same amount of intermetallic phase in each alloy, in equilibrium with α-Mg, and (b) single-phase α-Mg binary alloys (Mg-Zn and Mg-Y) containing the same solute amount as those in group (a). The result of hot deformation of the alloys in group (a) and (b) will reveal the effect of intermetallics and Y solute, respectively, on the texture evolution.

To determine the alloys group (a), the variation of the amount of intermetallics and composition of α-Mg as a function of Zn and Y content at 350 °C were calculated by FactSage™ software using the FTlite database [10]. Based on cost and density considerations, Zn amounts lower than 6 wt% and Y amounts lower than 2 wt% were considered for thermodynamic calculations. It was found that only two alloy compositions generate the same amount of different intermetallics in equilibrium with α-Mg that contains the same solute amount: Mg-5Zn-2Y and Mg-6Zn-1.2Y, in which the intermetallic phase in equilibrium with α-Mg at 350 °C is W ($Mg_3Y_2Zn_3$) and I (Mg_3YZn_6), respectively. The α-Mg in the mentioned alloys contains only Zn solute in equal amounts.

Experimental Procedure

High purity elements 99.9% Mg, 99.99% Zn, and 99.9% Y (all concentrations are given in wt% unless otherwise mentioned) were used to make the alloys by induction melting under the protective gas of SF_6 + CO_2. The melt was held at 740 °C for 30 min and stirred at regular intervals. The molten alloys were cast into rods 15 mm in diameter and 140 mm in height in a Cu mould pre-heated at 250 °C. Inductively coupled plasma atomic emission spectroscopy (ICP-AES) was used to determine the composition of alloys, which was close to the nominal one (− 0.1 wt% of maximum difference). The major impurity levels were 0.004 wt% for Si and Mn, and 0.03 wt% for Al and Fe. The as-cast alloys were initially heat treated at a temperature just below the liquid formation in heating of cast material, and then annealed at 350 °C which was chosen as the deformation temperature. The temperature of initial heat treatment was determined by simultaneous thermal analysis TG-DSC (Thermogravimetry-Differential Scanning Calorimetry) for melting of as-cast alloys heated at 10 K/min under Ar in pure iron crucible. All heat treatments were carried out in an air-circulating furnace with ±1 °C precision, followed by quenching the alloys into room-temperature water. The time required for heat treatment was obtained by measuring the variation of room-temperature Vickers macro hardness and the composition of Mg solid solution with time (2 h to 24 h). The latter was investigated by EPMA (electron probe micro-analysis in a JEOL JXA-8900L SEM) using 10 kV and MgO, $Y_3Al_5O_{12}$, and ZnS standards. Intermetallics were identified by EPMA (forty to fifty analyzed points) and bulk

X-ray diffraction (XRD) data. The latter was collected at room temperature with a Bruker D8 Advance diffractometer on a rotating and oscillating stage using a Cu $K\alpha$ source. Compositional contrast in backscattered electron (BSE) imaging was utilized to identify the form and distribution of intermetallics in a field emission gun SEM (FE-SEM Hitachi S-4700).

Compression tests on cylindrical samples (6 mm in diameter and 9 mm in height) were carried out under a steady argon flow at 350 °C (in a radiant furnace) and true strain rate of 1 s^{-1}. The samples were quenched in room-temperature water within 1 s after unloading at different strains (half of peak strain, peak strain, and strain of 1) or after annealing of deformed material. The post-deformation annealing was carried out immediately after unloading in the radiant furnace at 350 °C for 1 min to 30 min. The bulk texture was evaluated by XRD using a Bruker D8 diffractometer with a Co $K\alpha$ source. The orientation distribution function (ODF) was constructed from the incomplete pole figures of {10.0}, {00.2}, and {10.1}.

For microstructural examination, the samples were ground with 1200 grit SiC paper, and polished with 3 μm and 1 μm diamond suspension followed by 0.04 μm colloidal silica (Struers OP-S) polishing. The samples were then etched with acetic picral (10 ml acetic acid, 10 ml H_2O, 4.2 g picric acid, 70 ml ethanol) for 3 to 5 s. The grain sizes were measured using the linear intercept method based on ASTM E 112 standard, and the volume fractions of recrystallized material were determined using the point counting method from optical micrographs according to ASTM E 562 standard [15]. The deformed and recrystallized grains were differentiated based on their size and shape. The standard deviations are given in parenthesis, which refer to the last digit, e.g., 5.1(8) indicates 5.1 ± 0.8.

Results and Discussion

Alloy Design

BSE images show the presence of eutectic structure in as-cast alloys (Fig. 1).

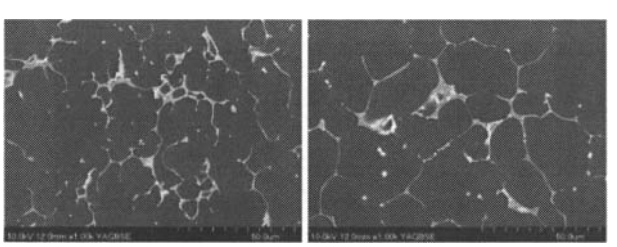

Figure 1. BSE image of the as-cast alloys Mg-6Zn-1.2Y (left) and Mg-5Zn-2Y (right).

Based on the results of XRD (Fig. 2) and EPMA (Zn/Y ratio was used to identify the intermetallics), the constituent phases in as-cast Mg-6Zn-1.2Y alloy are α-Mg and I phase (Zn/Y: 5.1(8) at%). The as-cast Mg-5Zn-2Y alloy is composed of α-Mg, I (Zn/Y: 5.4(8) at%) and W (Zn/Y: 1.5(1) at%) phases (Fig. 3).

The onset of melting, detected by simultaneous TG-DSC, occurs at 450 °C in both Mg-6Zn-1.2Y and Mg-5Zn-2Y as-cast alloys. The initial heat treatment of ternary alloys was therefore carried out at 430 °C just below this temperature.

Based on the results of XRD (Fig. 2) and EPMA, the I phase in as-cast Mg-6Zn-1.2Y alloy transforms completely to the W phase (Zn/Y: 1.7(1) at%) at 430 °C after the shortest time of 2 h, and the W phase remains in the microstructure after 24 h. The I phase forms again upon annealing of the heat treated alloy (430 °C-8 h) at 350 °C for 24 h. This indicates that either the kinetics of W to I phase transformation is slow or the equilibrium intermetallics at 350 °C are I and W phases. To verify this, the Mg-6Zn-1.2Y as-cast alloy was heat treated at 350 °C from 2 h to 24 h. The W phase forms again after 2 h and remains in the microstructure along with the I phase after 24 h. However, at 330 °C, no W phase was detected by XRD and EPMA after heat treatment for 2 h to 24 h.

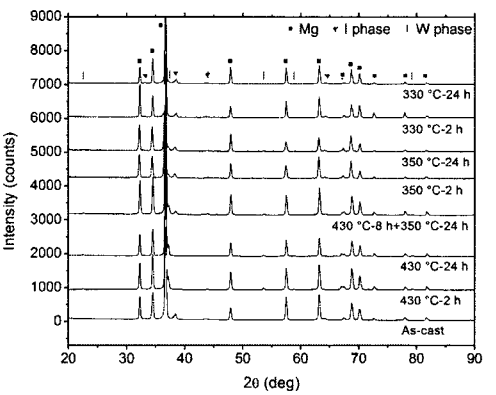

Figure 2. XRD patterns of Mg-6Zn-1.2Y alloy in the as-cast and heat treated states. Note that the most intense peaks of I and W phases are at 38.4° and 37.2°, respectively.

The intermetallic change from W phase, at 430 °C, to I phase, at 330 °C, could have beneficial effects on the texture evolution of deformed material. This alloy was therefore heat treated at 330 °C and 430 °C to obtain two distinct microstructures: α-Mg + I phase obtained at 330 °C (denoted by Mg-6Zn-1.2Y(I)), and α-Mg + W phase obtained at 430 °C (denoted by Mg-6Zn-1.2Y(W)).

As can be seen in the XRD patterns of Mg-5Zn-2Y alloy (Fig. 3), the I phase is not detected after heat treatment at 430 °C. Instead, the W phase is found at all tested times.

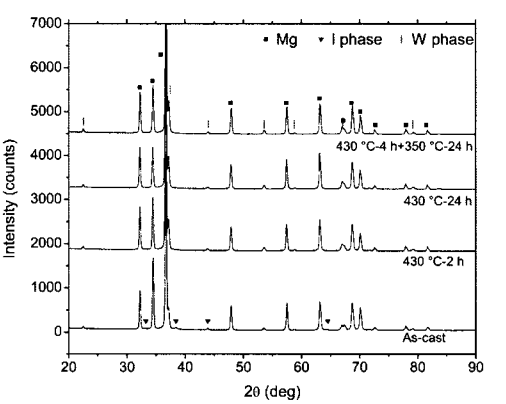

Figure 3. XRD patterns of Mg-5Zn-2Y alloy in the as-cast and heat treated states. Note that the most intense peaks of I and W phases are at 38.4° and 37.2°, respectively.

The minimum time of heat treatment, which was determined based on the onset of steady state regime in Vickers macro-hardness values and the amounts of Zn and Y solutes, was determined to be 8 h for Mg-6Zn-1.2Y alloy (at both temperatures 330 °C and 430 °C), and 4 h for Mg-5Zn-2Y alloy at 430 °C. The annealing of the heat treated Mg-5Zn-2Y alloy (430 °C-4 h) at 350 °C from 2 h to 24 h did not give rise to any change in the composition of α-Mg solid solution, macro hardness and microstructure. This alloy was therefore heat treated only at 430 °C for 4 h.

Since the intensity of X-ray peaks corresponding to intermetallics are low (due to their little amount), the volume percents of I and W phases were calculated by balancing the measured Zn amount, and are given in Table I. The density of I phase was taken from [16], and that of W phase was calculated from the crystal structure obtained by Rietveld refinement in [17]. The two binary alloys were selected based on the amount of Zn solute in Mg-6Zn-1.2Y (330 °C-8 h) and Mg-5Zn-2Y (430 °C-4 h) alloys, i.e, 2.9 wt%. The same procedure was undertaken for Mg-2.9Zn (1.1 at% Zn) and Mg-2.9Y (0.8 at% Y) alloys to find the temperature and time of heat treatment resulting in a fully solid solution microstructure at 350 °C. These binary alloys were therefore thermo-mechanically processed in the single-phase solid solution region, according to phase diagram data [12,13].

The heat treatment procedure and the characteristics of the four alloys explained above are summarized in Table I. It should be noted that the intermetallics in ternary alloys are in the form of interdendritic lamellar eutectic.

Table I. Heat treatment conditions and characteristics of the selected alloys. The standard deviations are given in parenthesis, which refer to the last digit.

Alloy (nominal composition in wt%)		**Mg-6Zn-1.2Y**		**Mg-5Zn-2Y**	**Mg-2.9Y**	**Mg-2.9Zn**
Heat treatment (T °C-t h)		330-8	430-8	430-4	430-24	430-8
Present phase(s)		α-Mg + I	α-Mg + W	α-Mg + W	α-Mg	α-Mg
Calculated amount of intermetallic*	**vol%**	1.68	1.24	2.01	–	–
	wt%	4.57	3.09	4.95	–	–
Predicted amount of intermetallic † (wt%)		7.32	I (6.94) + W (0.1)	6.85	–	–
Grain size (μm)		50(5)	51(7)	52(4)	124(12)	120(8)
Solute amount (wt%)	**Zn**	2.8(3)	4.7(2)	2.9(2)	–	2.8(1)
	Y	0.25(6)	0.10(6)	0.11(4)	2.8(2)	–

* Obtained by balancing the measured Zn amount
† Obtained by FactSage™ using FTlite database

Except for the Mg-6Zn-1.2Y alloy heat treated at 430 °C, the nature of the intermetallics predicted by thermodynamic calculations and obtained experimentally are similar. However, the amount of intermetallics obtained from experimental data appears to be lower than that predicted by thermodynamic calculations (Table 1).

Shao et al. [18] performed a recent assessment of the Mg-Zn-Y system, and generated a new database. Their database [18] was inputted in FactSage in this study to compare with the results obtained by the FTlite database. The result of thermodynamic calculations of the equilibrium phases for the alloys selected in this study revealed similar results from the two databases.

Hot Compression and Post-deformation Annealing

Since major texture changes occurred at the strain of 1, the following section includes the results of microstructure and texture study at this strain.

The typical basal texture develops in all alloys with nearly the same maximum intensity of basal pole figures (Fig. 4) at the strain of 1. It should be noted that the maximum error value in the maximum intensity of basal pole figures is ± 10%.

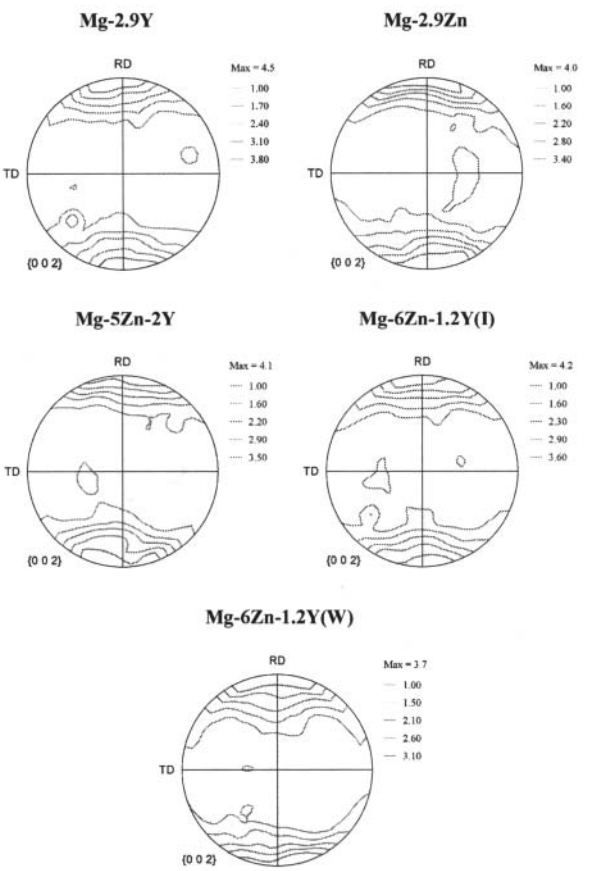

Figure 4. X-ray (00.2) basal pole figures after compression to the strain of 1. RD is the compression direction.

The noticeable anomaly in the microstructure of Mg-2.9Y alloy is the retardation of dynamic recrystallization (Fig. 5). While a nearly fully-recrystallized microstructure develops in all other alloys at strain of 1, the amount of recrystallized material in Mg-2.9Y is only 29(1) vol%.

The intermetallics in ternary alloys were observed to preserve their eutectic structure at peak strain, and deformed mostly into stringers at the strain of 1 (Fig. 6).

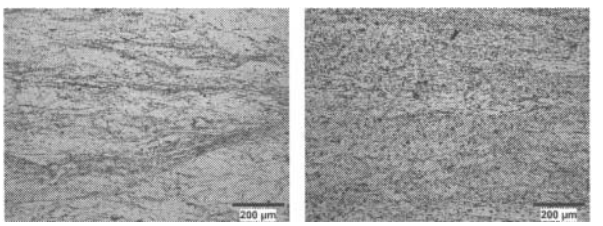

Figure 5. Optical micrographs showing the microstructures of Mg-2.9Y alloy immediately after compression to the strain of 1 (left) followed by 30-min annealing (right). The compression direction is parallel to the vertical direction on the micrographs.

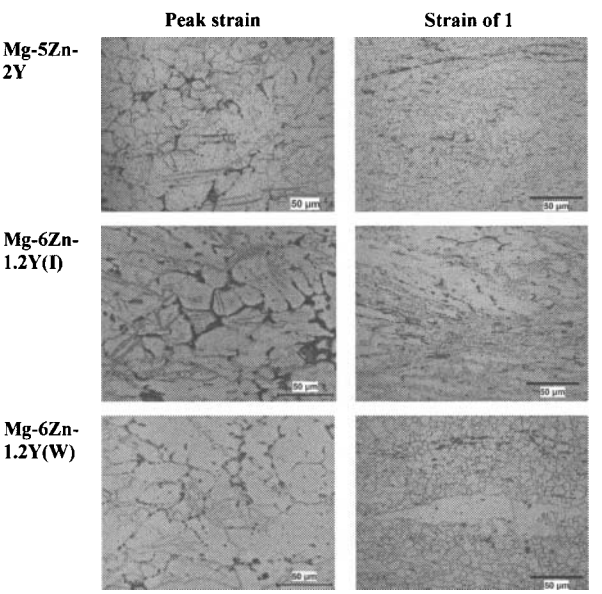

Figure 6. Optical micrographs showing the change in the form of intermetallics from eutectic structures at peak strain to stringers at the strain of 1.

Upon subsequent annealing of the compressed samples for 30 min, the maximum intensity of basal pole figures remains nearly unchanged, except in Mg-2.9Y alloy (Fig. 7). The texture evolution of Mg-2.9Y alloy with post-deformation annealing time is shown in Fig. 8 by inverse pole figures, illustrating the texture weakening in this alloy after sufficient annealing time (i.e., 30 min). It could therefore be concluded that the presence of the intermetallics investigated in this study does not have any beneficial effect in terms of texture weakening under the conditions investigated in this study.

The variation in volume percent (V_{rec}) and size (D_{RX}) of recrystallized grains with annealing time after strain of 1 in Mg-2.9Y alloy are given in Table II. Despite the large increase in V_{rec} after 1-min annealing (from 29(4) to 81(1) vol% in 1 min), the deformation texture remains nearly unchanged. However, after 30-min annealing, the texture weakening is accompanied by little rise in V_{rec} (from 81(1) to 94(1) vol%) and a large increase in D_{RX} (from 3.2(1) to 6.4(2) μm) with respect to 1-min annealing.

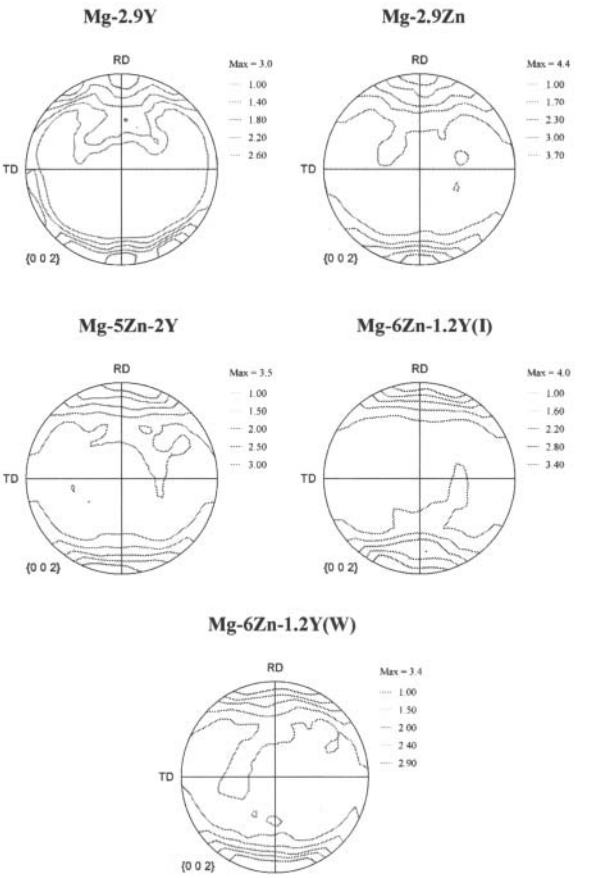

Figure 7. X-ray (00.2) basal pole figures of the alloys compressed to the strain of 1 followed by 30-min annealing. RD is the compression direction.

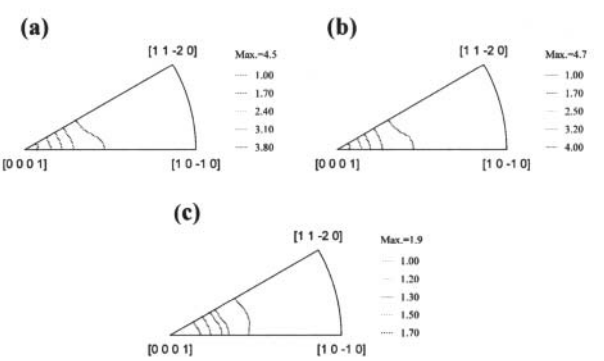

Figure 8. Result of X-ray texture measurement shown as IPF's referring to the compression direction in Mg-2.9Y alloy compressed to the strain of 1(a) and subsequently annealed (350 °C) for 1 min (b) and 30 min (c).

Table II. Volume percent (V_{rec}) and size (D_{RX}) of recrystallized grains with annealing time after strain of 1 in Mg-2.9Y alloy.

	No minutes	1 min	30 min
V_{rec}	29(4)	81(1)	94(1)
D_{RX}	2.0(2)	3.2(1)	6.4(2)

It could be concluded that the presence of Y in α-Mg solid solution can lead to texture weakening during the growth of recrystallized grains. It is hypothesized that a form of an orientation-dependent solute drag that could alter the mobility of specific high-angle boundaries could be responsible for the observed texture weakening in the Mg-2.9Y alloy.

Summary

The FactSage™ thermodynamic package was successfully used to select the alloys from Mg-Zn-Y system, aimed at determining the mechanism(s) of texture weakening in Y-containing Mg alloys.

The selected alloys are Mg-6Zn-1.2Y, Mg-5Zn-2Y, Mg-2.9Y and Mg-2.9Zn. After heat treatment, the ternary alloys contain (nearly) the same volume fraction of ternary intermetallics (I and W phases, respectively) in equilibrium with α-Mg at 350 °C, and the microstructure of the binary alloys is composed of α-Mg solid solution at 350 °C containing the same solute amount as that of Zn solute in the ternary alloys.

The results of hot deformation and post-deformation annealing of these alloys at a constant temperature (i.e., 350 °C) clarified the effect of Y in texture weakening of Mg. The obtained results show that the presence of Y in α-Mg solid solution can lead to texture weakening during the growth of recrystallized grains in deformed and annealed specimens.

Acknowledgements

The work described in this paper was supported in part by funding from the NSERC (Natural Sciences and Engineering Research Council of Canada) Magnesium Strategic Research Network. The author appreciates the financial support by the Werner Graupe International Fellowship from the Faculty of Engineering at McGill University. The assistance of Pierre Vermette with casting of the alloys is also gratefully acknowledged.

References

1. H.E. Friedrich, and B.L. Mordike, *Magnesium Technology, Metallurgy, Design Data, Applications* (Springer, 2006).

2. J. Bohlen, M.R. Nurnberg, J.W. Senn, D. Letzig, and S.R. Agnew, "The Texture and Anisotropy of Magnesium–Zinc–Rare earth Alloy Sheets," *Acta Materialia*, 55 (2007), 2101–2112.

3. J. Bohlen, J. Swiostek, D. Letzig, and K. Kainer, "Influence of Alloying Additions on the Microstructure Development of Extruded Mg-Mn Alloys," *TMS Magnesium Technology*, (2009), 225–230.

4. N. Stanford, and M. Barnett, "Effect of Composition on the Texture and Deformation Behavior of Wrought Mg Alloys," *Scripta Materialia*, 58 (2008), 179–182.

5. A. Hänzi, T. Ebeling, R. Bormann, and P. Uggowitzer, "New Microalloyed Magnesium with Exceptional Mechanical Performance," *TMS Magnesium Technology*, (2009), 521–526.

6. K. Hantzsche, J. Bohlen, J. Wendt, K.U. Kainer, S.B. Yia, and D. Letzig, "Effect of Rare Earth Additions on Microstructure and Texture Development of Magnesium Alloy Sheets," *Scripta Materialia*, 63 (2010), 725–730.

7. N. Stanford, "Micro-alloying Mg with Y, Ce, Gd and La for Texture Modification—A Comparative Study," *Materials Science and Engineering A*, 527 (2010), 2669–2677.

8. J. Wendt, K. Kainer, G. Arruebarrena, K. Hantzsche, J. Bohlen, and D. Letzig, "On the Microstructure and Texture Development of Magnesium Alloy ZEK100 During Rolling," *TMS Magnesium Technology*, (2009), 289–293.

9. Jeremy W. Senn, and Sean R. Agnew, "Texture Randomization of Magnesium Alloys Containing Rare Earth Elements," *TMS Magnesium Technology*, (2008), 153–158.

10. C.W. Bale, E. Bélisle, P. Chartrand, S.A. Decterov, G. Eriksson, K. Hack, I.-H. Jung, Y.-B. Kang, J. Melançon, A.D. Pelton, C. Robelin, and S. Petersen, "FactSage Thermochemical Software and Databases — Recent Developments", *CALPHAD*, 33 (2009), 295–311.

11. L.W.F. Mackenzie, and M.O. Pekguleryuz, "The Recrystallization and Texture of Magnesium-Zinc-Cerium Alloys," *Scripta Materialia*, 59 (2008), 665–668.

12. A.A. Nayeb-Hashemi, and J.B. Clarc, *Binary Alloy Phase Diagrams* (Second Edition, Ed. T.B. Massalski, ASM International, Materials Park, Ohio, 1990).

13. L.L. Rokhlin, *Magnesium Alloys Containing Rare Earth Metals* (London: Taylor & Francis, 2003).

14. R.W. Cahn, P. Haasen, and E.J. Kramer, *Materials Science and Technology* (Vol. 8, VCH, 1996), 151.

15. *ASTM Book of Standards*, Volume 03.01, Metals Test Methods and Analytical Procedures: Metals - Mechanical Testing; Elevated and Low-Temperature Tests; Metallography, 2009.

16. S. Bruhne, E. Uhrig, C. Gross, W. Assmus, A.S. Masadeh, and S.J.L. Billinge, "The Local Atomic Quasicrystal Structure of the Icosahedral $Mg_{25}Y_{11}Zn_{64}$ Alloy," *J Phys: Condens Matter*, 17 (2005), 1561–1572.

17. M. Sahlberg, and Y Andersson, "Hydrogen Absorption in Mg-Y-Zn Ternary Compounds," *J Alloys Compd*, 446–447 (2007), 134-137.

18. G. Shao, V Varsani, and Z. Fan, "Thermodynamic Modeling of the Y-Zn and Mg-Zn-Y system," *CALPHAD*, 30 (2006), 286-295.